Arabian Journal of Chemistry (2023) **16**, 104625

King Saud University

Arabian Journal of Chemistry

www.ksu.edu.sa
www.sciencedirect.com

ORIGINAL ARTICLE

Phytochemical components of Allium Jesdianum flower as effective corrosion-resistant materials for Fe(1 1 0), Al(1 1 1), and Cu(1 1 1): DFT study

Nuha Wazzan

King Abdulaziz University, Chemistry Department, Faculty of Science, P.O Box 42805 Jeddah 21589, Saudi Arabia

Received 26 November 2022; accepted 22 January 2023
Available online 25 January 2023

KEYWORDS

Allium Jesdianum;
Phytochemicals;
Green anticorrosive;
Monti Carlo simulation;
Adsorption

Abstract As anticorrosive materials, natural products such as flower extracts are widely used. In lieu of using the whole product, it is better to apply the isolated phytochemical active component among all existing components in the flower as anticorrosive. Therefore, identifying the component or components responsible for anticorrosion paves the road for its experimental synthesis and effective application. In the present investigation, a comprehensive investigation of three phytochemicals present in Allium Jesdianum (AJ) flower, namely Methyl heptadecanoate (Palmitic acid), Ethyl (9Z,12Z)-octadeca-9,12-dienoate (a-Linolenic acid), and Icosan-1-ol (1-Ecosanol) was characterized using computational methods (DMol3, and Monti Carlo (MC) simulations) to determine the inhibition potentials for corrosion, chemical reactivities, and adsorption behaviors. Isolated forms were characterized by local and global reactivity descriptors such as the energies and distributions of the highest occupied molecular orbitals (HOMOs), Lowest unoccupied molecular orbitals (LUMOs), their gaps, hardness (h), global softness (s), global electronegativity (χ), chemical potential (μ), electrophilicity (ω), nucleophilicity (ε), electron-accepting power (ω^-), electron-donating power (ω^+), and net electrophilicity ($\Delta\omega^{\pm}$). A further investigation has been made into the adsorption of three types of industrial metals, namely Fe(1 1 0), Al(1 1 1), and Cu(1 1 1). Based on the most stable adsorption configurations, the three phytochemicals adsorbed parallel to all surfaces. Adsorbate and surfaces interact primarily via chemisorption. In line with this result, the radial distribution function (RDF) has been analyzed. Computed parameters illustrated 1-Ecosanol's superiority over other phytochemicals and justified the reason behind its efficiency.

E-mail address: nwazzan@kau.edu.sa

Peer review under responsibility of King Saud University.

Production and hosting by Elsevier

https://doi.org/10.1016/j.arabjc.2023.104625

1. Introduction

As a result of corrosion, a person's health is at risk, and the problem is costly. There can be collapses of buildings and bridges, oil pipeline breaks, and chemical plant leaks. Fires and other issues can result from corroded electrical contacts and blood poisoning from corroded medical implants. As radioactive waste is stored in containers for tens of thousands of years, corrosion threatens its safe disposal. The search for green corrosion inhibitors has caught the attention of corrosion scientists in recent years (Kahkesh and Zargar, 2021; Singh, 2019; Prasad, 2022; Akalezi and Oguzie, 2016; Prasad, 2022; Abdellattif, 2021; Salleh, 2021; Elmsellem, et al., 2019; Hafez, 2019; Sikine, et al., 2016; Douche, 2020; Chkirate, 2021; Azgaou, 2022).

These inhibitors are biologically degradable, toxic-free, eco-friendly, and economical. Oxygen, nitrogen, sulfur, and multiple bonds in plant extracts provide inhibitory effects. Metal corrosion is prevented by physisorption and chemosorption from plant-derived corrosion inhibitors, which form protective films through electrostatic attraction or the formation of coordination bonds.

The properties of the inhibitor/surface mechanism and an understanding of the structural nature of the inhibitor in the corrosion process have been analyzed by quantum chemical calculations, especially density functional theory (DFT). Researchers can design promising inhibitor molecules and recognize their structures at an atomic level using DFT calculations. Therefore, DFT calculations can provide molecular-level insight into the most effective phytochemical/s in a plant extract. Efficient Phytochemical/s can then be synthesized in the laboratory and applied in the corrosion tests; by doing so, both time and the environment will be saved (Abdellattif, 2021).

Hafez et al. (Hafez, 2019) aimed to examine the effects of commercial oil of Eucalyptus on inhibition of corrosion with mild steel in HCl acid by means of potentiodynamic, gravimetric, polarization and electrochemical impedance spectroscopic techniques. It is found that the adsorption of Eucalyptus inhibitor follows the Langmuir adsorption isotherm equation. A direct relationship was found between the inhibition efficiency and immersion time of samples in the solution. Both the anodic metal dissolution and the cathodic hydrogen evolution acting as a mixed type of inhibitor as indicated from the polarization plots. In another effort by Fekkar et al. (Abdel-Rahman, 2020) the ethanol and hexane extracts of Chamaerops humilis L. fruits as green corrosion inhibitors for mild steel in 1.0 M HCl solution has been investigated. Corrosion rates were evaluated at 308 K using weight loss, potentiodynamic polarization and electrochemical impedance spectroscopy (EIS) techniques. Electrochemical techniques such as weight loss, electrochemical impedance spectroscopy (EIS) and potentiodynamic polarization showed that the extracts exhibit excellent inhibition efficiency. It was proved that the corrosion mechanism is controlled by charge transfer process and function as mixed type inhibitors. Langmuir adsorption isotherm was indicated. The inhibition efficiency increases with an increase in the concentration of the inhibitors and reaches not less than 80 %.

As a member of the Liliaceae family, Allium Jesdianum (AJ) grows widely in the west and northwest of Iran and is widely cultivated in Japan as a garden plant with purple-lilac flowers. There are many nutritional and medicinal uses for this plant. According to reports, AJ flowers contain three main phytochemicals tested by GC-Mass analysis. As a green anticorrosive for mild steel in an acidic solution, Kahkesh and Zargar (Kahkesh and Zargar, 2021) tested AJ extract. Using electrochemical impedance spectroscopy, the maximal inhibition efficiency was excellent and equaled 96.18 %. By potentiodynamic polarization, both cathodic and anodic corrosion current density declined, and mixed-type inhibition was confirmed. AJ extract concentration affects inhibition performance according to weight loss measurements, and Langmuir's adsorption isotherm describes banner adsorption on metal surfaces. However, in that study, the whole plant extract was used, so it was not possible to determine which phytochemical component was mostly responsible for the anticorrosive properties. To our knowledge, no theoretical work has been conducted to determine which phytochemical component of AJ is most effective as an anticorrosive agent. Abdellattif et al. (Abdellattif, 2021), through computational studies, investigated the most effective phytochemical inhibitors among the eight phytochemicals present in the Calotropis Procera plant. By force field COMPASS, it was possible to determine their orientation toward Fe(110) surface and to elucidate the three most active phytochemical inhibitors. Prasad et al. (Prasad, 2022), in a combined experimental and theoretical study, investigated Cinnamomum Tamala extract as an efficient bio-anticorrosive for low-carbon steel in 0.5 M H_2SO_4 solution. Several experimental techniques such as electrochemical impedance spectroscopy and Tafel and gravimetric loss, were applied to show that the inhibition efficiency of this extract reached 96.76 % at deficient concentrations. DFT and molecular dynamics (MD) simulations help in understanding the electronic adsorption and in performing a comparative inhibitory activity of phytochemicals.

As we can see from the above literature, as anticorrosive materials, natural products such as flower extracts are widely used. In lieu of using the whole product, it is better to apply the isolated phytochemical active component among all existing components in flower as anticorrosive. Therefore, identifying the component or components responsible for anticorrosion paves the road for its experimental synthesis and effective application. There will be a lot of savings for the

Table 1 A simulation of the adsorption of three phytochemical inhibitors on Fe (1110), Al (1111), and Cu (1110) in kcal/mol.

Inhibitor	**Fe(110)**				
	E_{tot}	E_{ads}	E_{rigid}	E_{def}	dE_{ads}/dN_i
GC1	–222.95	−182.35	−192.26	9.91	−182.35
GC2	−226.80	−195.62	−197.97	2.35	−195.62
GC3	−258.69	−203.19	−205.89	2.70	−203.19
	Al(111)				
	E_{tot}	E_{ads}	E_{rigid}	E_{def}	dE_{ads}/dN_i
GC1	−124.09	−83.48	−86.97	3.49	−83.48
GC2	−122.40	−91.21	−94.44	3.23	−91.21
GC3	−151.41	−95.91	−97.18	1.27	−95.91
	Cu(111)				
	E_{tot}	E_{ads}	E_{rigid}	E_{def}	dE_{ads}/dN_i
GC1	−134.41	−93.81	−96.19	2.39	−93.81
GC2	−132.60	−101.41	−105.22	3.80	−101.41
GC3	−163.82	−108.32	−109.64	1.33	−108.32

corrosion industry if corrosion inhibitors are developed to prevent corrosion of more than one metal at the same time (Wazzan et al., 2022). We were motivated by this to investigate the feasibility of the three phytochemicals present in AJ extract as effective environment-friendly inhibitors in acidic media for three metals: steel, aluminum, and copper. Fig. 1 presents the chemical structure and IUPAC names of these three phytochemical components. Through computational study outcomes, we seek to identify the most effective phytochemicals. Therefore, to examine the inhibition efficiency of three phytochemical constituents present in AJ extract in an acidic solution, we used Dmol3 and Monti Carlo (MC) simulations. Calculations based on DMol3/DFT showed the phytochemical' anticorrosive activity depends on its molecular structure. On Fe(1 1 0), Al(1 1 1), and Cu(1 1 1) metallic surfaces (surfaces with the greatest stability), a MC simulation method was used to study the orientations, adsorption energies, and radial distribution functions (RDFs) of the phytochemicals. Each molecule's major microspecies in 1 % HCl (pH = 0) were validated to be the ones presented in Fig. 1 and used in Dmol3 and MC simulations.

2. Method

A geometric form that could exist in an acidic medium was determined with the help of the MarvinSketch package. From the obtained result, the chemical structures of the three phytochemical active components in Allium Jesdianum in the acidic medium were proved to be the ones presented in Fig. 1. The subsequent calculations were then based on these structures.

2.1. Monti Carlo simulation details of adsorbed systems

The Monte Carlo (MC) simulation is one of the most potent techniques for simulating the adsorption of anticorrosive materials on metal surfaces (Khaled, 2009; Alamri, 2020; Kasprzhitskii and Lazorenko, 2021; Berisha, 2020). A Metropolis algorithm is used to implement the model (Metropolis, 1953). The MC simulation involves first cleaving bulk Fe, Al, and Cu metals into the Fe(1 1 1), Al(1 1 1), and Cu(1 1 1) surface with a thickness of 5.0 Å. In terms of thermodynamic stability, these surfaces ranked highest (Kokalj, 2010). The optimization processes of the resultant surfaces and the three investigated phytochemical inhibitors GC1-3 were detailed in our previous publication (Wazzan et al., 2022). Fe(1 1 1), Al(1 1 1), and Cu(1 1 1), these surfaces are five metallic layers. The size of the 3D Triclinic Fe(1 1 0) of a, b, and c are 24.82, 24.82, 38.18 Å, respectively, and 3D Triclinic Al(1 1 1) of a, b, and c are 28.63, 28.63, 39.44 Å, respectively, and the 3D Triclinic Cu(1 1 1) cell of a, b, c are 25.56, 25.56, 38.44 Å, respectively.(See Fig. 2).

2.2. DMol3 details of isolated inhibitors

Version 8.0 of Material Studio from BIOVIA was used to perform DFT calculations of isolated inhibitors using the DMol3 module. We are applying the generalized gradient approximation (GGA), a well-known algorithm. Many molecular systems naturally exhibit inhomogeneity in their electron gas, which GGA takes into account (Perdew, 1992; Becke, 1988), with PBE (Paier, 2005) and DNP basis set. Our previous publication provides details (Wazzan et al., 2022). COSMO was used to include the water solvent (Klamt, 2018). Ensure accurate results by setting all parameters to Fine. To achieve optimal geometry on potential energy surfaces, it is ensured that negative frequencies are absent from the obtained geometries.

3. Results and discussion

3.1. Adsorbed systems

As postulated by Kokalj (Kokalj, 2010), key factors determining inhibition effectiveness in corrosion inhibition studies are

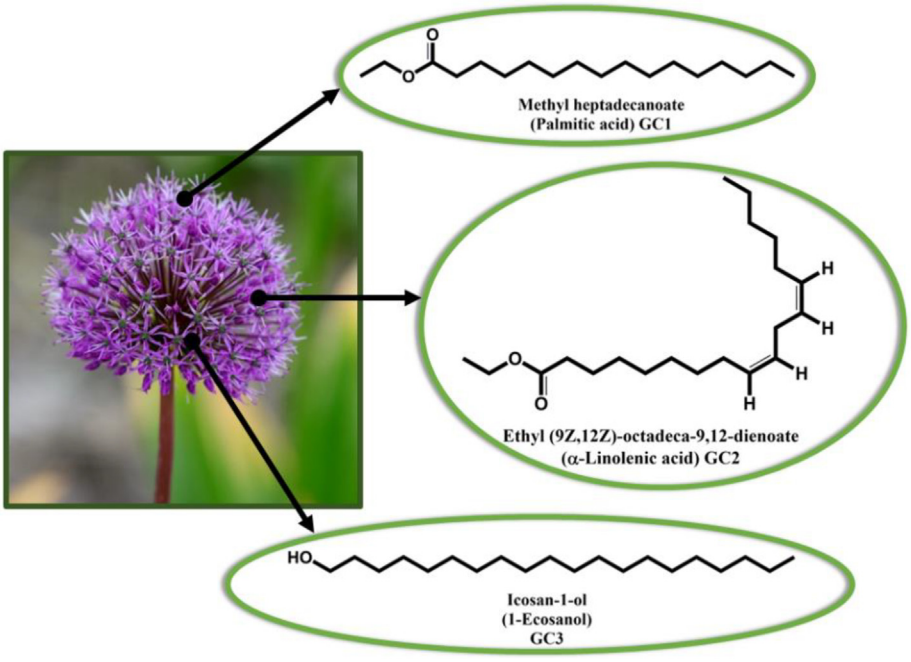

Fig. 1 The chemical structures of the active phytochemical components in Allium Jesdianum flower, along with their IUPAC names (common names) and abbreviations.

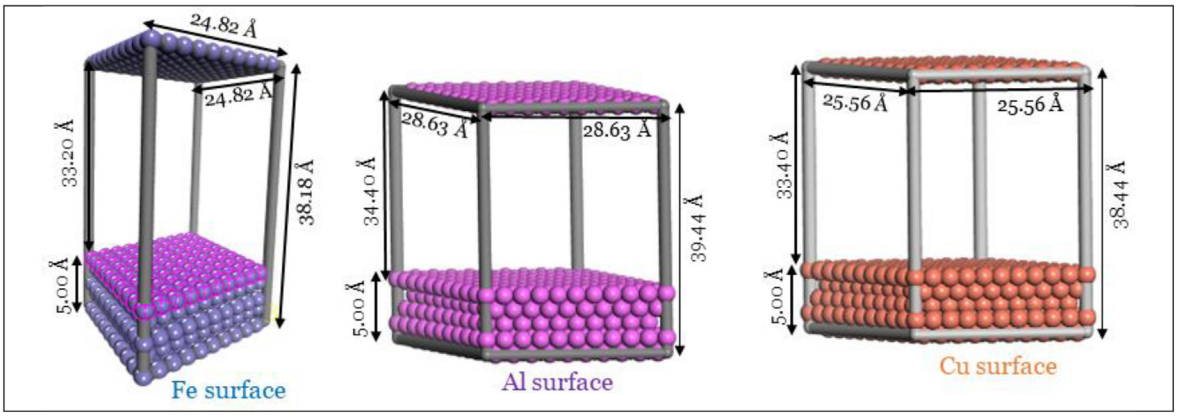

Fig. 2 Fe(1 1 0), Al(1 1 1), and Cu(1 1 1) periodic slab, along with the lattice parameters used in MC simulation.

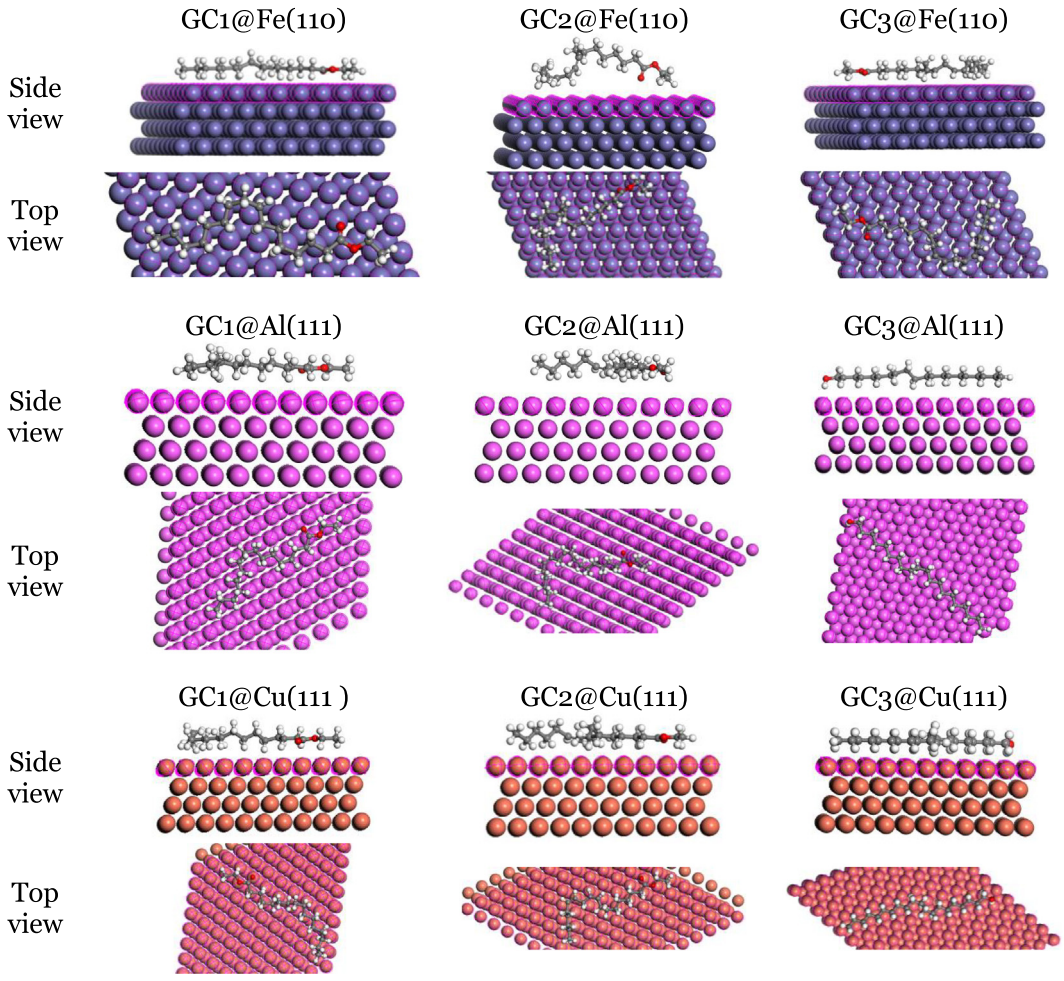

Fig. 3 The most stable adsorbed systems obtained from MC simulation.

carefully modeling the inhibitor-surface interaction and not the molecular electronic properties. Therefore, we will first look at the adsorption models of the three phytochemicals studied on the surface of the metal. Then, using the inhibitor's interaction with the metal surface (Fe(1 1 1), Cu(1 1 1), and Al (1 1 1)) serves as a tool for estimating the adsorption energies, this can be quantified as follows:

$$E_{ads} = E_{inh@Fe(111)/Al(111)/Cu(111)} - \left(E_{Fe(111)/Al(111)/Cu(111)} + E_{inh}\right) \quad (1)$$

Where $E_{inh@Fe(111)/Al(111)/Cu(111)}$ is the total energy of the simulated corrosion system, and $E_{Fe(111)/Al(111)/Cu(111)}$ is the total calculated energy of the Fe(1 1 1), Al(1 1 1), and Cu(1 1 1) surfaces and that of the E_{inh} is the total calculated energy of the

free inhibitor molecule. Our MC simulation enabled us to determine the ideal adsorption site for the metal surface using the adsorption locator model. In Fig. 3, the simulated acidic corrosion media, the three studied phytochemicals displayed the most stable (lowest energy) configurations. A representative image of phytochemical inhibitor molecule orientation is obtained through MC simulation. As a result, it is possible to determine if inhibitor molecules with similar orientations to metal will offer better corrosion inhibition protection, i.e., when the corrosion inhibitor has a flat orientation, it covers a larger surface area and provides more corrosion inhibition protection than when it has a vertical orientation (Singh, 2019). Since phytochemicals acquire a horizontal or flat positioning, they covering a large metallic surface, helping to adsorb them to the three metal surfaces (Abdellattif, 2021; Berisha, 2020; Singh, 2019). While GC1 and GC3 have relatively larger surface areas, better surface coverage and protection is provided by them.

The minima calculated energies (kcal/mol) (Table 1) that were found at the best adsorption site: (i) the total energy (substrate/adsorbate energy, E_{tot}), (ii) rigid adsorption energy (unrelaxed adsorbate components adsorbed on the substrate, E_{rigid}), (iii) deformation energy (relaxed adsorbate components adsorbed on the substrate, E_{def}), (iv) adsorption energy (rigid adsorption energy + deformation energy, E_{ads}), and (v) (dE_{ads}/dN_i) (metal–inhibitor energy, where one of the inhibitor molecules has been removed) (Elgendy, 2019). Here are the results of the simulation of the adsorption of the three inhibitors on Fe(1 1 0), Al(1 1 1), and Cu(1 1 1) surfaces using MC listed in Table 1, and the adsorption energies are plotted in Fig. 4. According to Equation (1), the inhibitor covers the metal surface with a protective layer based on the negative adsorption energy. The adsorption energies of inhibitors on the Fe(1 1 1), Cu(1 1 1), and Al(1 1 1) are all negative and in the range from −83.48 to −203.19 kcal/mol. In general, molecules attach to metal surfaces via chemosorption since higher adsorption energies make chemosorption more effective (Wazzan et al., 2022; Kasprzhitskii and Lazorenko, 2021; El-Aouni, 2021). A study of the adsorption energies of inhibitors on the Fe(1 1 0) revealed that they are significantly larger than those on Cu (1 1 1) and Al(1 1 1), where the values for the last two metals are somehow comparable. Compared to Cu(1 1 1) and Al (1 1 1), the inhibitors form a more stable protective layer on Fe(1 1 0). On the other hand, GC3 shows the highest adsorption energies, followed by GC2 and GC1 for the three metals. According to this observation, GC3 is the most active anticorrosive phytochemical in Allium Jesdianum flower in an acidic medium.

3.1.1. Radial distribution function

It is possible to gain a further understanding of the interactions between phytochemical inhibitor molecules and metal surfaces by analyzing radial distribution functions (RDFs). An important indicator of inhibitor interaction with metal surfaces is the first prominent peak in the RDF curve. Because physical interactions tend to produce peaks of greater than 3.5 Å, whereas peaks between 1.0 Å and 3.5 Å indicate chemisorption (Xie, 2015). MD simulation trajectories were used to determine the total radial distribution function of the three phytochemical inhibitors (Fig. 5).

From Fig. 5, we can see that the first peaks of the three phytochemical inhibitors appear at 2.87 Å, 2.55 Å, and 2.54 Å in Al(1 1 1), Cu(1 1 1), and Fe(1 1 0), regardless of the type of inhibitor molecule. The bond length between the metal surface inhibitor is less than 3.5 Å, indicating a chemosorption interaction. Additionally, the strength of interaction with the three metals increases as follows: Al(1 1 1) < Cu(1 1 1) < Fe(1 1 0). This order of the strength of interaction ($g(r)$ vs r curve) comes very consistent with the order of increasing the adsorption energies.

3.2. Isolated inhibitors

3.2.1. Frontier molecular orbitals and energy gaps

Inhibitor molecules are reacted chemically with metal surfaces through the highest occupied (HOMO) and lowest unoccupied

Table 2 Calculated molecular quantum chemical descriptors (MQCDs) of the investigated phytochemical inhibitors.

QCPs	Inhibitor		
	GC1	GC2	GC3
E_{HOMO}(/eV)	−6.173	−5.440	−5.964
E_{LUMO}(/eV)	−0.653	−0.668	1.521
Energy gap, ΔE_{gap} (/eV)	5.520	4.772	7.485
Ionization energy, $I = -E_{HOMO}$ (/eV)	6.173	5.440	5.964
Electron affinity, $A = -E_{LUMO}$ (/eV)	0.653	0.668	−1.521
Global hardness, $h = \frac{I-A}{2}$(/eV)	2.760	2.386	3.743
Global softness, $s = \frac{1}{h}$(/eV^{-1})	0.362	0.419	0.267
Global electronegativity, $\chi = -\frac{I+A}{2}$ (/eV)	3.413	3.054	2.222
Chemical potential, $\mu = -\chi$ (/eV)	−3.413	−3.054	−2.222
Electrophilicity, $\omega = \frac{\mu^2}{4h} = \frac{I+A}{8(I+A)^2}$ (/eV)	2.110	1.955	0.659
Nucleophilicity, $\varepsilon = \frac{1}{\omega}$ (eV^{-1})	0.474	0.512	1.517
Electron accepting power, $\omega^- = \frac{(3I+A)^2}{16(I-A)}$(/eV)	4.162	3.780	2.238
Electron donating power, $\omega^+ = \frac{(I+3A)^2}{16(I-A)}$(/eV)	22.815	16.527	0.918
Net electrophilicity, $\Delta\omega^{\pm} = \omega^+ + \omega^-$(/eV)	26.976	20.307	3.156
Total energy change, ΔE_{B-D}(/eV)	−0.690	−0.597	−0.936

(LUMO) molecular orbitals. Two processes dominate the interaction between the metal surface and the inhibitor molecule. The two processes are: electrons are donated from the inhibitor molecule to the empty d-orbital of the metal (transition metal), and electrons are given back to the inhibitor molecule from the filled d-orbital. Therefore, the two processes complete each other, and both benefit enhancing the adsorption process. The ability of the inhibitor molecule to donate an electron to the metal surface is measured by the energy of the HOMO orbital (E_{HOMO}), as the E_{HOMO} becomes high (less negative; destabilized) as the donation process becomes more accessible. Accordingly, its ionization energy ($I = -E_{HOMO}$) should be small in value. In contrast, inhibitor molecules' ability to accept an electron from the metal surface is measured by the energy of its LUMO orbital (E_{LUMO}), as the E_{LUMO} becomes low (more negative; stabilized) as the accepting process becomes easier. Accordingly, its electron affinity ($A = -E_{LUMO}$) should be large in value. A molecule with such HOMO-LUMO alignment is chemically soft. In accordance with the HSAB principle, bulk metals are chemically the softest of all materials, so they interact better with soft materials.

In addition, the HOMO-LUMO energy gap ($\Delta E_{gap} = E_{LUMO} - E_{HOMO}$) should be as small as possible to indicate a more reactive inhibitor molecule toward the anticorrosive behavior. Table 2 and Fig. 6 show the optimized geometries, energies of HOMOs and LUMOs, gaps, and special distributions in an aqueous medium. Simulation in the aqueous medium is essential as the corrosion of the metals occurs in the hummed environment.

The results from Table 2 and Fig. 6 show that the E_{HOMO} values increase (less negative; destabilized) in the following order: GC1 < GC3 < GD2, and thus the ability to donate electrons would be predicted following the same order. While the E_{LUMO} values decrease (more negative; stabilized) in the following order: GC3 < GC1 < GD2, and thus the ability to accept electrons would be predicted following the same order. In contrast, the ΔE_{gap} values of GC1 and GC2 are small equal 3.468 and 5.520 eV, respectively, and thus indicate the ease of polarization of these two investigated phytochemical molecules. ΔE_{gap} values decrease in the following order: GC3 > GC1 > GC2, and thus the reactivities of the inhibitor molecules will follow the reverse order. We should mention here that a smaller ΔE_{gap} value, however, as Kokalj and coworkers demonstrate, it does not unambiguously indicate a better inhibitor (Kokalj, 2021).

Inspection of the special distribution of electron density of HOMOs and LUMOs is essential to the qualitative determination of which part/s of the molecule are capable of donating/

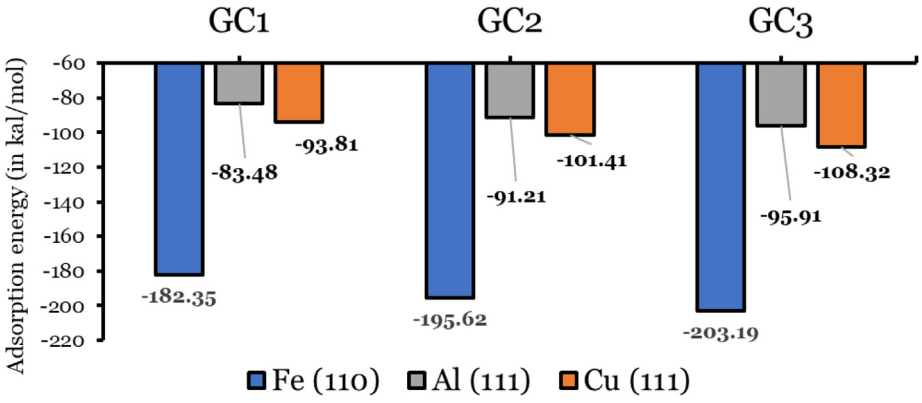

Fig. 4 MC simulations of the adsorption energies (in kcal/mol).

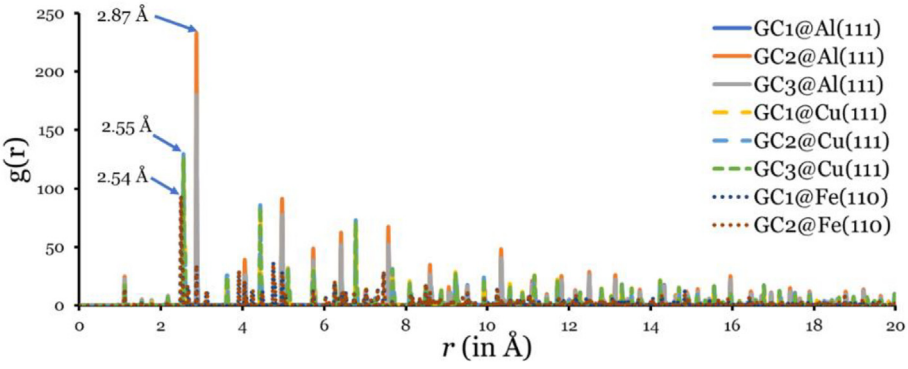

Fig. 5 RDFs of investigated phytochemical inhibitors adsorbed on the metal surfaces.

accepting electrons. The hydrocarbon parts of GC1 and GC3 seem unreactive to donate or accept electrons since any HOMOs and LUMOs do not occupy them. The HOMOs and LUMOs are delocalized mainly on the terminal alcoholic unit in GC3 and the ester unit in GC1. In GC2, part of the hydrocarbon chain can donate electrons since the HOMO orbital is delocalized over it. At the same time, the ester unit can accept electrons since the LUMO orbital is delocalized over this part of the molecule.

3.2.2. Molecular quantum chemical descriptors

Hard and soft acids and bases (HSAB) theories can explain the reactivity of three phytochemical molecules toward metal surface adsorption (Pearson, 1963; Geerlings et al., 2003). According to HSAB principal, several molecular quantum chemical descriptors (MQCDs) such as global hardness (h), global softness (s), global electronegativity (χ), chemical potential (μ), electrophilicity (ω), nucleophilicity (ε), electron-accepting power (ω^-), electron-donating power (ω^+), and net electrophilicity ($\Delta\omega^{\pm}$) can be evaluated. Detailed equation used to evaluate these descriptors can be found next to each descriptor in Table 2.

Global hardness is synonymous with the ΔE_{gap} apart from the factor of ø (Kokalj, 2021). On the other hand, upon contact between inhibitor and metal, there will be a flow of electrons from lower χ (inhibitor) to higher χ (metal) until the chemical potentials becomes matched. Sanderson's electronegativity equalization principle says that the inhibitor with a large electronegativity difference will require a longer time to reach equalization. This will lead to a high level of reactivity, which implies a high level of inhibition (Geerlings and De Proft, 2002). Therefore, low global hardness and electronegativity values suggest that phytochemical inhibitors are highly reactive molecules capable of accepting and transferring electrons during the interaction between metals and inhibitors (Dagdag, 2020). Among the three molecules, GC2 is the softest molecule ($h = 2.386$ eV), and GC3 has the smallest χ value (2.222 eV). Electro- and nucleophilicity descriptors indicate the inhibition molecule's ability to accept and donate electrons.

A charge transfer model for donation and back-donation charges make up another essential descriptor, i.e., the total energy change (ΔE_{B-D}). Based on the value of the molecular hardness, as shown in the following equation, the charge transfer model can be calculated:

$$\Delta E_{B-D} = -\frac{h}{4} \tag{2}$$

Thus, it is suggested that if $h > 0$ or $\Delta E_{B-D} < 0$, the electron back-donation from the metal surface to the empty orbitals of inhibitor molecules is energetically favorable. ΔE_{B-D} are negative, and the maximum value is −0.936 eV for GC3, indicating the stronger charge back-donation to this inhibitor.

Among the three phytochemical molecules, GC3 has the lowest ω and the largest ε values, showing that the molecule is more likely than the other two to give electrons to the empty d-orbital of the metal surface. On the other hand, GC1 has the largest ω and the lowest ε values. The tendency of GC1 to accept electrons from the occupied d-orbital of the metal exceeds that of the other two molecules. We can conclude that the adsorption mechanism involves the transport of electrons

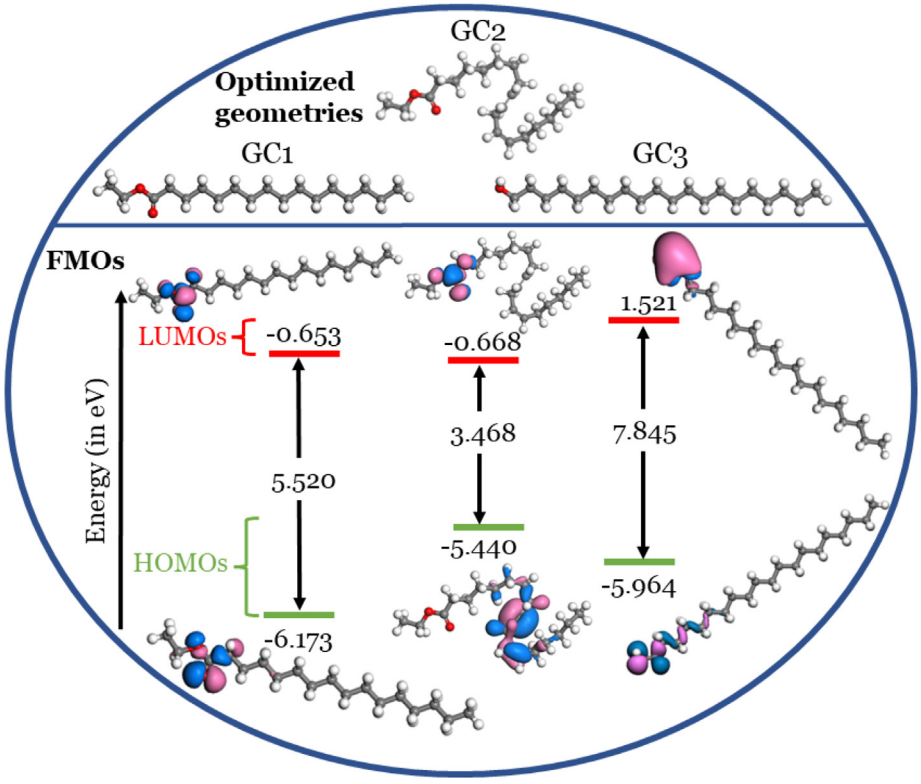

Fig. 6 Densities of HOMOs and LUMOs, their energies and energy gaps (in eV) in aqueous medium. Note: Isovalue: 0.03 au.

from the inhibitor to the metal surface in light of the adsorption behavior of the three molecules on the three metal surfaces.

3.2.3. Local Fukui functions

A local Fukui function in inhibitor molecules could reveal nucleophilic (f^+) and electrophilic (f^-) attack sites (Fukui, 1982). Fig. 7 presents the 3D plots of the isosurfaces of the three investigated phytochemical inhibitors with nucleophilic and electrophilic Fukui functions in water. There is no domination of the distribution of electrophilic and nucleophilic Fukui functions on the molecular skeletons of the three investigated inhibitors. For GC1 and GC3, the f^+ and f^- functions are delocalized on the same sections of the molecule, i.e., ester in GC1 and alcoholic unit in GC3. Therefore, these sites are responsible for both electrophilic and nucleophilic attacks. Conversely, the existence of an ester unit in GC2 does not mean that it is the site for both attacks. Since it is where f^+ function is relocated, and therefore electrophilic attack occurs at this site, electrophilic attack occurs at this site, whereas nucleophilic attack occurs at the branched alkene since it is occupied by f^- function.

3.2.4. Inhibitor-metal interactions descriptors

When assessing the phytochemical inhibitor's interaction with a specific metal, the inhibitor-metal interaction descriptors are necessary, and they are listed in Table 3. Such descriptors included the number of transferred electrons (ΔN) from the inhibitor to the metallic surface. Based on the obtained values of χ and h, ΔN value can be calculated (Parr and Pearson, 1983):

$$\Delta N = \frac{(\chi_{metal} - \chi_{inh})}{2(h_{metal} + h_{inh})} \quad (3)$$

Electron transfer is driven by electronegativity difference, and resistance is determined by the sum of hardness parameters (Khalil et al., 2016). According to the free electron gas model, the values of electronegativity are related to the Fermi energy of metal in free-electron gases. As a result, electron–electron interactions are ignored. As for the metal surface, the workfunction (φ_{metal}) is taken as its electronegativity (Kovačević and Kokalj, 2011). Thus, φ_{metal} of the metal has been incorporated, so the electronegativity measurement is at the appropriate level. In contrast, a lack of attention is paid to chemical hardness since bulk metals have relatively low Fermi state levels, and their hardness is determined by the density of those states (Yang and Parr, 1985). Thus ΔN value can be expressed as follows:

$$\Delta N = \frac{(\varphi_{metal} - \chi_{inh})}{2h_{inh}} \quad (4)$$

The experimental values of φ_{metal} for bulk metals are: 4.82, 4.24, and 4.98 eV for Fe, Al, and Cu metals, respectively (Michaelson, 1977). If $\Delta N > 0$, inhibitor molecule is donor and metal is acceptor and if $\Delta N < 0$, the reverse is true. With greater electron-giving capacity at the metal surface, inhibition efficiency also increased, i.e., $\Delta N < 3.6$, according to Lukovits. The computed electronegativities of the three phytochemical inhibitors are 3.413 eV (GC1), 3.054 eV (GC2), and 2.222 eV (GC3). All are smaller than the workfunctions of metals, so ΔN is positive. The inhibitor molecule will flow electrons to the metal more readily than the metal will flow electrons to the inhibitor molecule (Kokalj, 2010). The most electrons were transferred for all metals by GC3, then GC2, and then GC1,

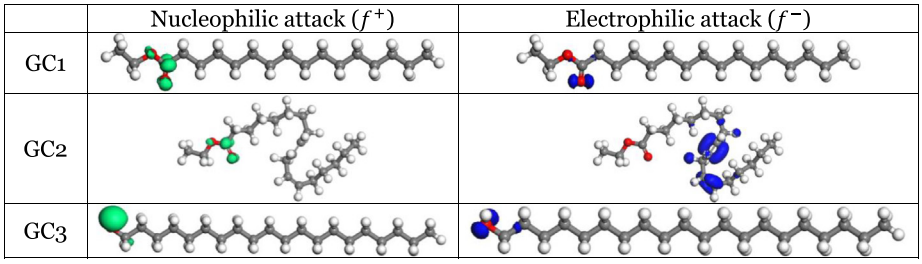

Fig. 7 3D plots of isosurface for the electrophilic and nucleophilic Fukui functions in an aqueous solution (Isovalue: 0.03 au).

Table 3 Calculated inhibitor-metal interactions descriptors of the invistigated phytochemical inhibitors obtained from the DMol3/ method.

QCPs	Fe(111)			Al(111)			Cu(111)		
	GC1	GC2	GC3	GC1	GC2	GC3	GC1	GC2	GC3
Number of transferred electrons, ΔN (/e)	1.942	2.107	4.862	1.141	1.415	3.777	2.162	2.298	5.162
Initial molecule–metal interaction energy,$\Delta\psi$ (/eV)	1.366	1.860	6.318	0.472	0.839	3.812	1.694	2.213	7.119
free energy of adsorption, ΔG_{ads} (cathodic) (in kJ/mol)	135.8	170.4	250.7	79.8	114.4	194.8	151.2	185.8	266.2
free energy of adsorption, ΔG_{ads} (anodic) (in kJ/mol)	−135.8	−170.4	−250.7	−79.8	−114.4	−194.8	−151.2	−185.8	−266.2

according to the order of adsorption strength on metal surfaces. On the other hand, inhibitors and metal types also affect the number of electrons transferred.

Another essential descriptor is the initial molecule–metal interaction energy ($\Delta\psi$). $\Delta\psi$ is an estimate of the initial molecule–metal interaction energy, which is given by the following equation:

$$\Delta\psi = \frac{(\chi_{metal} - \chi_{inh})^2}{4(h_{metal} + h_{inh})} = \frac{(\varphi_{metal} - \chi_{inh})^2}{4h_{inh}} \quad (5)$$

The conclusion for $\Delta\psi$ values is in the same vein as the one derived for ΔN values. Calculating the adsorption free energy (ΔG_{ads}) is a way to understand the adsorption mechanism (chemisorption or physisorption). If the metal Fe/Al/Cu would act as an anode, the inhibitor would serve as a cathode. The value of ΔG_{ads} can be determined according to the following equations:

$$\Delta G_{ads}(\text{cathodic}) = \chi_{(Fe/Al/Cu)} - \chi_{inh} = \varphi_{(Fe/Al/Cu)} - \chi_{inh} \quad (6)$$

$$\Delta G_{ads}(\text{anodic}) = \chi_{inh} - \chi_{(Fe/Al/Cu)} = \chi_{inh} - \varphi_{(Fe/Al/Cu)} \quad (7)$$

Similarly to what was perfumed earlier, their workfunctions will replace the electronegativities of metals. The values of ΔG_{ads} of the three investigated phytochemical inhibitors are listed in Table 3. Values of $\Delta G_{ads} \gg \pm 40$ kJ/mol, clearly indicating chemosorption as the adsorption mechanism. As for the three metals, ΔG_{ads} values of GC3 are much greater than those of GC1 and GC2, followed by GC2 and then GC1, this result is very consistent with MC simulations of their adsorption trend.

4. Conclusions

In this work, DMol3 and MC simulations were applied to investigate the best anti-corrosive material among the three phytochemical components (GC_i (i = 1–3)) in AJ flower for Fe(1 1 0), Al(1 1 1), and Cu (1 1 1) metals. MC simulation revealed through the values of adsorption energies and peaks in RDFs that the inhibition effect of the three investigated compounds increased in the order GC1 < GC2 < GC3. The DFT outputs from the DMol3 simulation show consistent results with the trend approved by MC simulation for most calculated parameters. This study indicated the responsibility of GC3 for the inhibition effect of this flower for more than one metal.

5. Availability of data

The author confirms that the data supporting this study's findings are available within the article and its supplementary data.

Declaration of Competing Interest

The authors declare that they have no known competing financial interests or personal relationships that could have appeared to influence the work reported in this paper.

Acknowledgment

In this paper, the author acknowledges King Abdulaziz University's High-Performance Computing Centre (Aziz Supercomputer) for supporting the computations. Furthermore, for support with the Materials Studio software, the author is grateful to Prof. Ime Bassey Obot from the interdisciplinary Research Center for Advanced Materials, King Fahd University of Petroleum and Minerals, Dhahran 31261, Saudi Arabia.

References

Abdellattif, M.H. et al, 2021. Calotropis procera extract as an environmental friendly corrosion Inhibitor: computational demonstrations. J. Mol. Liq. 337, 116954.

Abdel-Rahman, I., et al., Eco-friendly Chamaerops humilis L. fruit extract corrosion inhibitor for mild steel in 1 M HCl. 2020. **9**: p. 446-459

Akalezi, C.O., Oguzie, E.E., 2016. Evaluation of anticorrosion properties of Chrysophyllum albidum leaves extract for mild steel protection in acidic media. Int. J. Industrial Chem. 7 (1), 81–92.

Alamri, A.H., 2020. Experimental and theoretical insights into the synergistic effect of iodide ions and 1-acetyl-3-thiosemicarbazide on the corrosion protection of C1018 carbon steel in 1 M HCl. Materials 13 (21), 5013.

Azgaou, K. et al, 2022. Synthesis and characterization of N-(2-aminophenyl)- 2-(5-methyl-1H-pyrazol-3-yl) acetamide (AMPA) and its use as a corrosion inhibitor for C38 steel in 1 M HCl. experimental and theoretical study. J. Mol. Struct. 1266, 133451.

Becke, A.D., 1988. Density-functional exchange-energy approximation with correct asymptotic behavior. Phys. Rev. A 38 (6), 3098–3100.

Berisha, A., 2020. Experimental, Monte Carlo and molecular dynamic study on corrosion inhibition of mild steel by pyridine derivatives in aqueous perchloric acid. Electrochem 1 (2), 188–199.

Chkirate, K. et al, 2021. Corrosion inhibition potential of 2-[(5-methylpyrazol-3-yl)methyl]benzimidazole against carbon steel corrosion in 1 M HCl solution: combining experimental and theoretical studies. J. Mol. Liq. 321, 114750.

Dagdag, O. et al, 2020. Highly functionalized epoxy macromolecule as an anti-corrosive material for carbon steel: computational (DFT, MDS), surface (SEM-EDS) and electrochemical (OCP, PDP, EIS) studies. J. Mol. Liq. 302, 112535.

Douche, D. et al, 2020. Anti-corrosion performance of 8-hydroxyquinoline derivatives for mild steel in acidic medium: gravimetric, electrochemical, DFT and molecular dynamics simulation investigations. J. Mol. Liq. 308, 113042.

El-Aouni, N. et al, 2021. Performance of two new epoxy resins as potential corrosion inhibitors for carbon steel in 1MHCl medium: combining experimental and computational approaches. Colloids Surf. A Physicochem. Eng. Asp. 626, 127066.

Elgendy, A. et al, 2019. Understanding the adsorption performance of two glycine derivatives as novel and environmentally safe anti-corrosion agents for copper in chloride solutions: experimental, DFT, and MC studies. RSC Adv. 9 (72), 42120–42131.

Elmsellem, H., et al. A NATURAL ANTIOXIDANT AND AN ENVIRONMENTALLY FRIENDLY INHIBITOR OF MILD STEEL CORROSION: A COMMERCIAL OIL OF BASIL (OCIMUM BASILICUM L.). 2019.

Fukui, K., 1982. Role of frontier orbitals in chemical reactions. Science 218 (4574), 747–754.

Geerlings, P., De Proft, F., 2002. Chemical reactivity as described by quantum chemical methods. Int. J. Mol. Sci. 3 (4), 276–309.

Geerlings, P., De Proft, F., Langenaeker, W., 2003. Conceptual density functional theory. Chem. Rev. 103 (5), 1793–1874.

Hafez, B. et al, 2019. Environmentally friendly inhibitor of the corrosion of mild steel: commercial oil of Eucalyptus. Int. J. Corros. Scale Inhib. 8, 573–585.

Kahkesh, H., Zargar, B., 2021. Corrosion protection evaluation of Allium Jesdianum as a novel and green source inhibitor for mild steel in 1M HCl solution. J. Mol. Liq. 344, 117768.

Kasprzhitskii, A., Lazorenko, G., 2021. Corrosion inhibition properties of small peptides: DFT and Monte Carlo simulation studies. J. Mol. Liq. 331, 115782.

Khaled, K.F., 2009. Monte Carlo simulations of corrosion inhibition of mild steel in 0.5 M sulphuric acid by some green corrosion inhibitors. J. Solid State Electrochem. 13 (11), 1743–1756.

Khalil, S., Al-Mazaideh, G., Ali, N., 2016. DFT calculations on corrosion inhibition of aluminum by some carbohydrates. Int. J. Biochem. Res. Rev. 14, 1–7.

Klamt, A., 2018. The COSMO and COSMO-RS solvation models. WIREs Comput. Mol. Sci. 8 (1), e1338.

Kokalj, A., 2010. Is the analysis of molecular electronic structure of corrosion inhibitors sufficient to predict the trend of their inhibition performance. Electrochim. Acta 56 (2), 745–755.

Kokalj, A. et al, 2021. How relevant are molecular electronic parameters for predicting corrosion inhibition efficiency: imidazoles as corrosion inhibitors of Cu/Zr materials in NaCl solution. Corros. Sci. 193, 109900.

Kovačević, N., Kokalj, A., 2011. DFT study of interaction of azoles with Cu(111) and Al(111) surfaces: role of azole nitrogen atoms and dipole-dipole interactions. J. Phys. Chem. C 115 (49), 24189–24197.

Metropolis, N. et al, 1953. Equation of state calculations by fast computing machines. J. Chem. Phys. 21 (6), 1087–1092.

Michaelson, H.B., 1977. The work function of the elements and its periodicity. J. Appl. Phys. 48 (11), 4729–4733.

Paier, J. et al, 2005. The Perdew–Burke–Ernzerhof exchange-correlation functional applied to the G2–1 test set using a plane-wave basis set. J. Chem. Phys. 122, (23) 234102.

Parr, R.G., Pearson, R.G., 1983. Absolute hardness: companion parameter to absolute electronegativity. J. Am. Chem. Soc. 105 (26), 7512–7516.

Pearson, R.G., 1963. Hard and soft acids and bases. J. Am. Chem. Soc. 85 (22), 3533–3539.

Perdew, J.P. et al, 1992. Atoms, molecules, solids, and surfaces: applications of the generalized gradient approximation for exchange and correlation. Phys. Rev. B 46 (11), 6671–6687.

Prasad, D. et al, 2022. De-scaling, experimental, DFT, and MD-simulation studies of unwanted growing plant as natural corrosion inhibitor for SS-410 in acid medium. Physicochemical and Engineering Aspects, Colloids and Surfaces A, p. 129333.

Prasad, D. et al, 2022. Cinnamoum tamala leaves extract highly efficient corrosion bio-inhibitor for low carbon steel: applying computational and experimental studies. J. Mol. Liq. 347, 118218.

Salleh, S.Z. et al, 2021. Plant extracts as green corrosion inhibitor for ferrous metal alloys: a review. J. Clean. Prod. 304, 127030.

Sikine, M., et al., Inhibition Study of Mild Steel Corrosion in Hydrochloric Acid by 1, 5- Benzodiazepine-2,4-dione. 2016: p. 1386-1395.

Singh, A. et al, 2019. Effect of electron donating functional groups on corrosion inhibition of J55 steel in a sweet corrosive environment: experimental, density functional theory, and molecular dynamic simulation. Materials 12 (1), 17.

Singh, A. et al, 2019. Investigation of corrosion inhibitors adsorption on metals using density functional theory and molecular dynamics simulation, in Corrosion Inhibitors. IntechOpen London, UK.

Wazzan, N., Obot, I.B., Fagieh, T.M., 2022. The role of some triazoles on the corrosion inhibition of C1020 steel and copper in a desalination descaling solution. Desalination 527, 115551.

Xie, S.-W. et al, 2015. Molecular dynamics simulation of inhibition mechanism of 3,5-dibromo salicylaldehyde Schiff's base. Comput. Theor. Chem. 1063, 50–62.

Yang, W. and R.G. Parr, Hardness, softness, and the fukui function in the electronic theory of metals and catalysis. Proceedings of the National Academy of Sciences, 1985. **82**(20): p. 6723-6726.